


Influence of the grain boundary character on the temperature of transition to complete wetting in the Cu–In system

Alexander B. Straumal^{1,2}  · Victoria A. Yardley³ · Boris B. Straumal^{1,2,4} · Alexei O. Rodin²

Received: 25 November 2014 / Accepted: 15 April 2015 / Published online: 28 April 2015
© Springer Science+Business Media New York 2015

Abstract The incomplete to complete grain boundary (GB) wetting transition is controlled by GB energy and, therefore, by GB character. To find the GB character dependence of the wetting transition, experiments were carried out on polycrystalline Cu–In alloys, which are known to exhibit wetting behaviour between 715 and 986 °C. Electron backscatter diffraction was applied to determine the two-dimensional GB character, using the coincidence site lattice (CSL) model and applying the Brandon criterion. Special wetting behaviour was found in those GBs characterised as low-angle, $\Sigma 3$ and $\Sigma 11$. The low-angle and $\Sigma 3$ GBs were not wetted until the sample melted, while the temperature for the transition to complete wetting of $\Sigma 11$ GBs was over 100 °C higher than that for complete wetting of all other types of GB, including other CSL GB as well as random GB. It might be that a different Brandon type criterion is needed in the case of GB wetting to show the “special” wetting behaviour of the CSL GBs.

Introduction

Grain boundary wetting transition

Wetting phenomena are widely encountered and extremely important in processes ranging from liquid-phase sintering to oil recovery or melt infiltration [1–4]. If a two- or multicomponent polycrystal is partially melted, i.e. at a temperature between the solidus temperature T_S and the liquidus temperature T_L , then, for a given fraction of liquid phase, the spatial distribution of this phase between the solid grains depends on the wetting energetics of grain boundaries (GB) [5, 6]. The GB can be completely, incompletely or not at all wetted. In the first of these cases, the GB separating the grains is completely substituted by two solid–liquid interfaces and the contact angle θ between the GB and the melt is zero ($\theta = 0^\circ$) (Fig. 1a). In the second case, the GB co-exists with the liquid phase and the contact angle between GB and melt is finite ($\theta > 0^\circ$) (Fig. 1b). Cahn [7] and Ebner and Saam [8] first showed that a (reversible) transition from incomplete to complete wetting could occur on increasing the temperature and that this could be considered as a surface phase transformation. For a given grain boundary, the temperature of the transition to complete wetting, T_w , depends on both the GB energy σ_{GB} and the energy of the solid–liquid interfaces σ_{SL} . T_w is the temperature at which $2\sigma_{SL}$ becomes equal to σ_{GB} as shown in Fig. 1c. These two energies depend on the crystallography of the interfaces [9–12]. Wetting experiments on bicrystals, in which the GB misorientation and plane orientation are exactly known, allow highly accurate measurement of the dihedral contact angle θ [5, 6]. In this case, θ is measured in the section perpendicular to the flat individual GB and to the straight contact line between the GB and the liquid phase. In bicrystals, wetting

✉ Alexander B. Straumal
alexander.straumal@rub.de

¹ Present Address: Institute of Solid State Physics, Russian Academy of Sciences, Ac. Ossipyan str. 2, 142432 Chernogolovka, Russia
² National University of Science and Technology MISiS, Leninskii prosp. 4, 119049 Moscow, Russia
³ Ruhr-Universität Bochum, Universitätsstr. 150, 44801 Bochum, Germany
⁴ Moscow Institute of Physics and Technology (State University), Institutskii per. 9, 141700 Dolgoprudny, Russia

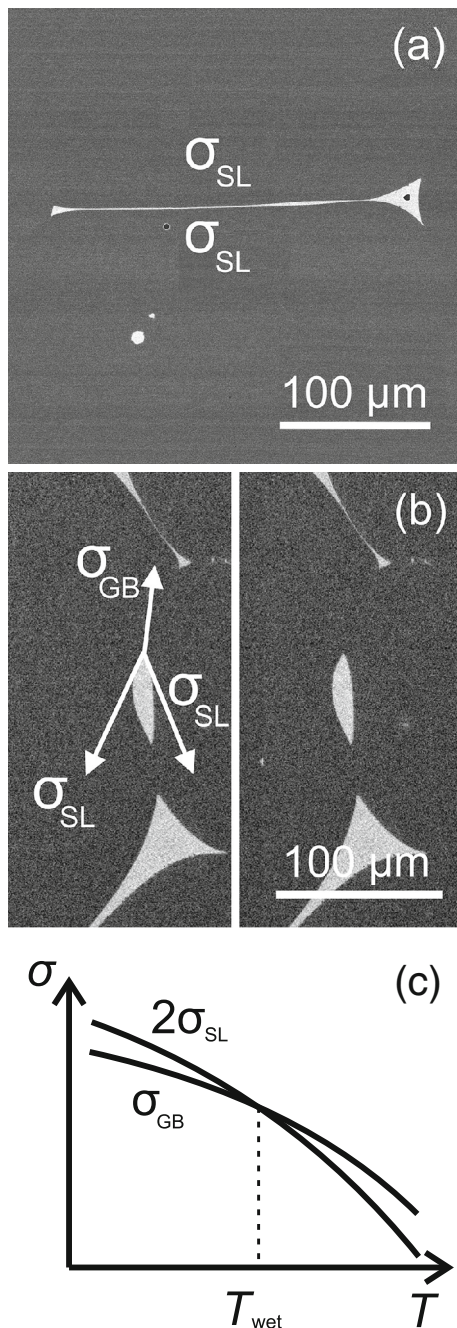


Fig. 1 **a** A typical wetted GB in Cu–In alloy; the GB between two wetted triple junctions is substituted by a complete layer of the second liquid phase (*bright horizontal line* on the picture) with two solid/liquid interface boundaries; the two σ_{SL} —energies of the solid/liquid interface boundaries indicate that there is no GB left and that the substituted GB does not contribute to the total energy of the system any more. **b** A typical non-wetted grain boundary in Cu–In alloy; the wetting layer of the second liquid phase is not complete and builds a contact wetting angle; the size of the wetting angle shows the geometrical equilibrium of the two σ_{SL} —energies of the solid/liquid interface boundaries and the GB energy σ_{GB} shown by the vectors on the picture. **c** The graph of the temperature dependences of boundary energies; the lines for the $2\sigma_{SL}$ and the σ_{GB} intersect at the wetting temperature T_w where the system is more likely to substitute a GB by a complete layer of the second phase with two solid/liquid interface boundaries to lower its total energy

these temperatures have been determined with the aid of conventional light microscopy or SEM for many systems exhibiting wetting [13–18]. This earlier work did not, however, consider how the wetting temperatures of individual GB were correlated with parameters describing their crystallographic characteristics. Wynblatt and Takashima [19, 20] made electron backscatter diffraction (EBSD) observations with serial sectioning on a single incompletely wetted sample of an Fe-30 wt% Mn-10 wt% Cu alloy in order to correlate the wetting state with the 5-parameter grain boundary character and thereby validate their model of grain boundary energy. In the present work, in contrast, we investigate the temperature of transition from incomplete to complete wetting and its dependence on grain boundary character using a series of Cu–In samples annealed at different temperatures.

There are several variables that can be measured to characterise a wetting phase transition and its relationship to GB geometry. These are the dihedral contact angle θ (as in Fig. 1b), the wetting state (completely wetted, incompletely wetted or non-wetted) and the GB character of the wetted or non-wetted GBs. All these variables must be measured at all temperatures up to the melting temperature in the case of liquid-phase wetting or up to the point where the grains are melting faster than the GBs left non-wetted.

In polycrystals, the contact angle θ is rather difficult to determine. If a GB contains lenticular liquid droplets, these are bounded by two spherical solid/liquid interfaces. The correct θ value appears only in the section containing the common axis of both spherical solid/liquid interfaces. It can be measured either using transmission electron microscopy [12] or by careful three-dimensional analysis of the droplet shape [21, 22]. If such methods are not practical due to the large numbers of boundaries to be characterised, then the wetting state is instead evaluated by analysing the appearance of the wetting layers of the second phase and categorising them as either completely, incompletely or not

behaviour can thus be correlated with the full three-dimensional macroscopic description of the grain boundary, consisting of three parameters characterising misorientation and two describing the orientation of the grain boundary plane. In polycrystalline samples, the transition from incomplete to complete GB wetting starts at a certain minimum temperature T_{wmin} at GB with a combination of maximum σ_{GB} and minimum σ_{SL} , and finishes at a maximum temperature T_{wmax} corresponding to a combination of minimum σ_{GB} and maximum σ_{SL} . In the previous work,

at all wetted. This is the method most commonly used for wetting experiments in polycrystalline materials. A full description of the macroscopic geometry of a grain boundary comprises five degrees of freedom, two of which characterise the orientation of the grain boundary plane. This is difficult, if not impossible, to determine on a two-dimensional section, and since the serial-sectioning methods required for three-dimensional characterisation are time-consuming it has become customary in grain boundary engineering work to describe the boundary geometry in terms of only three parameters describing the misorientation between the grains, and to relate this to the coincidence site lattice (CSL) model [23] using a tolerance criterion such as that proposed by Brandon [24]. In the present work, we investigate whether the temperature of transition from incomplete to complete wetting correlates with the CSL-based grain boundary character, categorising boundaries according to their reciprocal density of coincident sites Σ or as low-angle or random high-angle boundaries. The Brandon criterion [24] was used to determine whether a GB with a structure close to a CSL position should be considered as a CSL boundary.

There is also information in literature that at certain temperatures the CSL GBs lose their “specialness” and become “general” [25]. This needed to be investigated in the case of wetting behaviour of special GBs.

Materials and methods

Material

The Cu–In system has been chosen for this investigation because it is known that the GB wetting phase transition exists in this system [26] and values for T_{wmin} and T_{wmax} have already been determined [13]. According to the results of [13], the sample compositions were chosen to minimize the effect of the apparently complete wetting. To investigate the real Cahn wetting, the equilibrium fraction of liquid in the system had to be between 0 and 0.15. Cu–In alloys with 4, 8, 12 and 16 wt% indium were prepared from high-purity components (5N8 Cu and 5N6 In) by vacuum induction melting and casting into 10-mm-diameter rods. Slices of 2-mm thickness were cut from these ingots and sealed into evacuated silica ampoules with a residual pressure of approximately 4×10^{-4} Pa at room temperature. After the samples were sealed in ampoules, they were heat treated to homogenize the microstructure.

Annealing treatment

Samples were annealed at temperatures between 712 and 992 °C for 2 h (each individual sample is represented by a

grey point on Fig. 2), and then quenched in water. The accuracy of the annealing temperature was estimated to be ± 2 °C. The annealing treatments were performed in the two-phase (Cu) + L area of the Cu–In phase diagram [27], where the term (Cu) represents a Cu-based fcc solid solution. Combinations of temperature and composition were chosen based on the work in [13] such that the equilibrium fraction of liquid in the system was between 0 and 0.15. In the temperature range from 712 to 732 °C, additional annealing treatments were carried out on Cu-16 % In samples with a step size of 2 ± 0.5 °C (shown in the Fig. 2 by the writing “8 points” as the points sit too tight at the scale chosen for the figure). This allowed us to capture wetting temperatures of GB that are wetted just above the peritectic transformation temperature.

The choice of the annealing time of 2 h was made to ensure that an equilibrium state had been reached in all samples. To verify the homogeneous distribution of copper and indium in the matrix phase, EDX mapping was performed. Figure 3a–c shows an EDX map of a fragment of the microstructure of the sample with 16 wt% indium after annealing at 712 ± 0.5 °C for 2 h and quenching. It is clear from Fig. 3b, c that the composition of the copper-based solid solution (Cu) (the large grains in Fig. 3a–c) is homogeneous. The distribution of the elements in the second, grain boundary phase is not homogeneous, although the inhomogeneity is on smaller scales than are easily visible using the EDX scan resolution on the SEM. At the temperature of the wetting anneal, the second phase

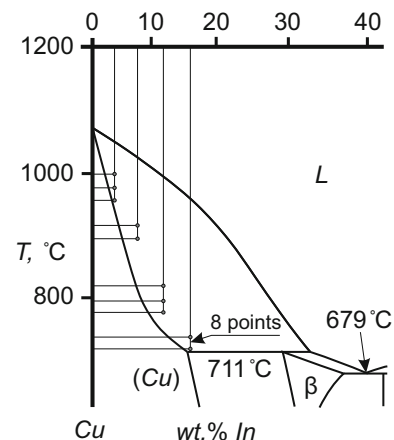


Fig. 2 The upper left part of the Cu–In phase diagram; the investigated two-phase area is the L (liquid) + (Cu) (copper-based solid solution of indium in copper) two-phase area of the peritectic β to L + (Cu) transformation; the filled circles show the annealing points and the horizontal and vertical lines show the respective annealing temperatures and compositions. For clarity, the additional annealing points for Cu-16 wt% In in the temperature range from 712 to 732 °C (accuracy of ± 0.5 °C and a step size of 2 °C between the points) are indicated by the arrow labelled “8 points”, as the scale is too big to show each point in the figure

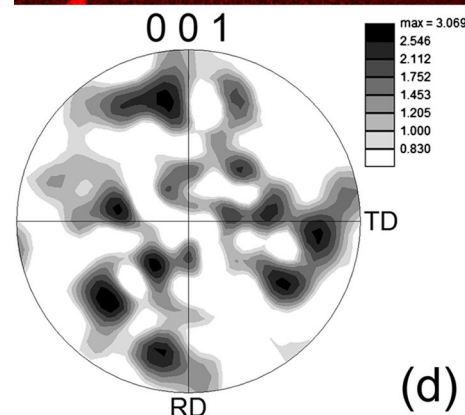
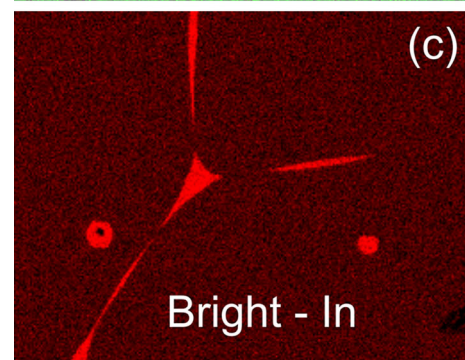
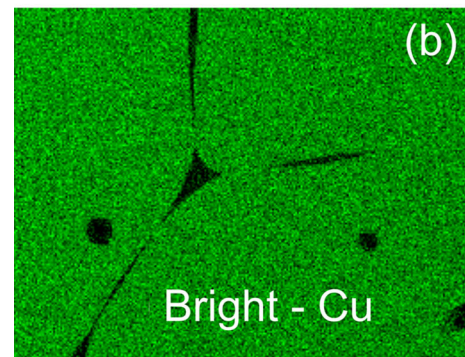
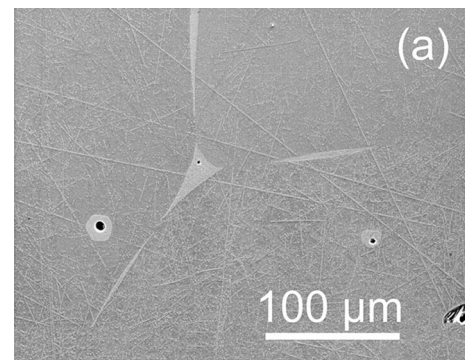
is liquid, but the quenching rate is not high enough to transform the liquid into an amorphous phase, and instead a peritectoid forms in the volume previously occupied by the liquid phase. Figure 3d shows a $\{001\}$ orientation distribution function (ODF) image, obtained using the EBSD analysis software discussed below, of the crystal orientations found in the microstructure of the same sample on an area of 1 mm^2 at a magnification of 100. The figure with ODF maxima of three reveals a weak (if any) texture. In [28], the initial sample state had a ODF maxima of 4.69 which is even higher than in our case, so we can reasonably expect to see a distribution of grain boundary character that is a reflection of the properties of the (Cu) phase, rather than of some specific thermomechanical processing history of this phase.

Metallographic preparation

After quenching, samples were embedded in electroconductive resin and then mechanically ground and polished, using $0.05 \text{ }\mu\text{m}$ SiO_2 suspension and an automatic vibratory polisher in the last polishing step.

Scanning electron microscopy (SEM)

Polished samples were then investigated using a LEO 1530 VP scanning electron microscope (SEM) equipped with an orientation imaging system from TSL. The EBSD method allows us to make spatially coupled crystallographic analyses of the polycrystalline sample surface showing the crystallographic orientation of each grain; an example is shown in Fig. 4a [29]. Four high-resolution EBSD scans were made for each sample in order to obtain a sufficiently large number of GB for statistical analysis. Each scan covered an area of at least $1000 \times 1000 \text{ }\mu\text{m}^2$. With a maximum step size of $1 \text{ }\mu\text{m}$ and a minimum of 10^6 points, it took about 12 h to acquire a full dataset. The chosen EBSD parameters were required to resolve thin twins. The wetting layers on the GB can be $<0.5 \text{ }\mu\text{m}$ thick. Since crystallographic data from these layers were not required in the present study, and since mapping them in EBSD would necessitate a reduced step size and consequently an increase in the number of points in the already large EBSD datasets, high-resolution BSD images of the same areas were used to study the morphology of the wetting layers. BSD gives good phase contrast between the indium-rich wetting layers and the copper-rich grains, but does not usually show any contrast at twin boundaries, as can be seen by comparison of Fig. 4a, b. Both EBSD and BSD data were thus required to investigate the dependence of wetting behaviour on grain boundary character.



Analysis

A quantitative analysis of wetting was performed adopting the following criterion: every boundary between (Cu) grains was considered to be completely wetted only when a

Fig. 3 **a** Fragment of the microstructure of the sample Cu-16 wt% In after annealing at 712 ± 0.5 °C for 2 h and quenching; the *bright triangle* in the middle is a wetted triple junction with three bright lenses of the second phase on the not completely wetted GBs connected in this triple junction. **b** EDX mapping of the copper concentration of the same fragment; the second phase in the triple junction and on the GBs is almost *black* as the copper concentration in the matrix copper-based solid solution phase is much higher than in the second liquid phase. **c** EDX mapping of the indium concentration of the same fragment; the second phase in the triple junction and on the GBs is *light grey* as the indium concentration is high. **d** Orientation distribution function (ODF) of the crystal orientations in the same sample; there is no ordering seen in the picture of the ODF maxima and the intensities of the ODF maxima are very low so only a weak (if any) texture is present in the sample and the section direction of the sample does not affect the result of the experiments

layer of indium-rich film had covered the whole GB; if such a layer appeared to be interrupted, the GB was regarded as incompletely wetted; boundaries with no layer present were classed as non-wetted. Since the purpose of this study was to investigate the temperature of transition from incomplete to complete wetting, a binary classification was used, in which the incompletely wetted and non-wetted boundaries were grouped together in a single category (wetting state 0) while the completely wetted boundaries were assigned the wetting state 1. At least 1000 GB were analysed in each sample. To determine the character of the grain boundaries, the misorientation between each pair of neighbouring grains was calculated using the TSL OIM Analysis six software (EDAX Ltd.) using point-by-point analysis. Each grain boundary was then classified based on the CSL model [23], applying the Brandon criterion [24].

Results

GB character distribution

According to the GB classification used, the GB character distribution encountered in the polycrystalline sample was determined (Table 1). As can be seen, the majority, 72.7 %, of GBs had random high misorientation angles. $\Sigma 3$ CSL boundaries have a fraction of 8.6 %, low-angle grain boundaries, 5.9 % and $\Sigma 5$ CSL boundaries, 1.2 %. Grain boundaries with all other Σ values from 7 to 49 had a frequency of <1 %. The mean number of GB used in statistical analysis per sample was 1820 (minimum 1000, maximum 4000), such that a 1 % fraction represents only 18 boundaries on average. It is therefore clear that the wetting graphs and temperatures should be treated with some caution if the fraction of the boundary in question is lower than 1 %.

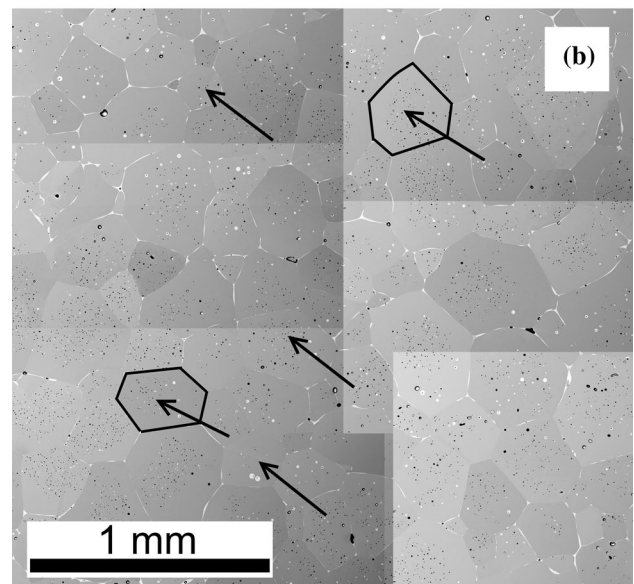
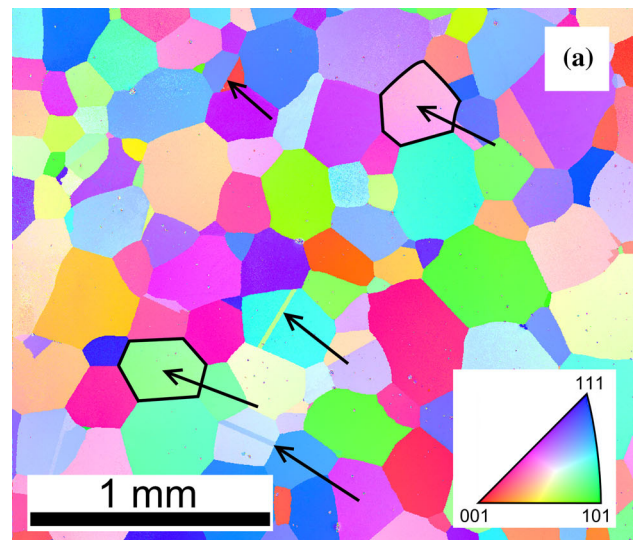


Fig. 4 Typical SEM results for polycrystalline Cu-16 wt% In alloy. **a** Orientation image map (normal direction, inverse pole figure); all GBs are clearly seen; arrows are showing identical areas on **(a, b)**. **b** Corresponding backscatter micrograph; the grains between the twin boundaries and the non-wetted GBs are almost or not visible but the second wetting phase is clearly visible

Wetting temperatures

Figure 5 shows the temperature dependences of the wetted GB fractions of “all GB” (representing the whole dataset), “random high misorientation angle GB”, “low misorientation angle GB” and $\Sigma 3$ CSL boundaries.

Figure 5 also shows experimental points for the high misorientation angle random GBs; the error bars are large because the wetting state of the GB was simply defined as “0” or “1” with no intermediate values. The only way to decrease the standard deviation and thus the size of the

Table 1 Grain boundary character distribution and maximal wetting temperatures

GB character	Frequency (%)	T_{wmax} (°C)
$\Sigma 3$	8.56	Not reached
$\Sigma 5$	1.17	819
$\Sigma 7$	0.98	811
$\Sigma 9$	0.90	805
$\Sigma 11$	0.80	947
$\Sigma 13$	0.75	836
$\Sigma 15$	0.85	803
$\Sigma 17$	0.48	n/a
$\Sigma 19$	0.56	805
$\Sigma 21$	0.74	811
$\Sigma 23$	0.49	n/a
$\Sigma 25$	0.43	n/a
$\Sigma 27$	0.47	n/a
$\Sigma 29-49$	4.16	n/a
Low-angle random GBs	5.94	Not reached
High-angle random GBs	72.72	825
Mean number of GB per sample		1820

error bars is to increase the number of GB analysed. However, we consider that the trends in wetting behaviour are sufficiently clear from Fig. 5.

An asymptotic function with a maximum value of 1 was fitted to the experimental points for all chosen types of GB using OriginPro 8.5G in order to estimate the T_{wmax} values for these types of boundaries.

The error bars show that if there are no non-wetted GBs of this type found in the sample this does not mean that they can't exist in another section of the sample. They also indicate that if a line reaches saturation close to the value 1, the GBs represented by this data could all be completely wetted as the non-wetted fraction of the GBs could be of a completely different type with lower GB energy due to the uncertainties of the 2D EBSD.

The random high misorientation angle GBs are all completely wetted at 825 °C. In contrast, the low misorientation angle and $\Sigma 3$ CSL boundaries are not all completely wetted in the temperature range of the two-phase area examined. Only at the melting temperature of the system the low misorientation angle GB line gets close to the value 1. If we sum up the random high misorientation angle GB, random low misorientation angle GB and $\Sigma 3$ and other CSL boundaries, the resulting “all GB” curve does not reach a fraction of 1.0 due to the contribution of the incompletely wetted GB (overwhelmingly low-angle and $\Sigma 3$). The curves for all other GB types (not shown on Fig. 5) have a similar appearance to the curve for the random high misorientation angle boundaries. The temperatures for complete wetting of each of these boundary types are shown in Table 1.

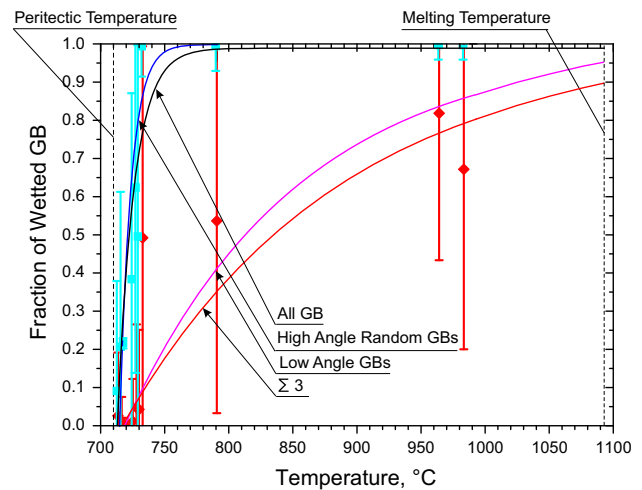


Fig. 5 Temperature dependence of the number fraction of completely wetted grain boundaries; four rising asymptotic lines show the wetting tendency of all GBs; the lines for random high misorientation GBs and for all GBs reach saturation at values 1 and 0.988 respectively; the lines for low misorientation angle GBs and the CSL $\Sigma 3$ boundaries cross the graph area much lower than the first two and do not reach any kind of saturation until the melting temperature. Experimental points for the high misorientation angle random GBs (square shaped points) and for CSL $\Sigma 3$ GBs (diamond shaped points) are given to supplement the choice of the asymptotic function as the fitting function for the experimental data

As is shown in Fig. 5, the “all GB” curve reaches a saturation value of 0.988 at 867 °C. This is the maximum wetting temperature T_{wmax} for “all GB” in the apparently complete wetted Cu–In system. In the previous work, the maximum wetting temperature T_{wmax} for “all GB” was defined as 986 °C [13].

Overview of the wetting temperature intervals

The distribution of T_{wmin} and T_{wmax} values for all GB types encountered in the system is represented in Fig. 6 (note the inversion of the temperature scale, for reasons that will be discussed below). The large grey area represents the interval between T_{wmin} and T_{wmax} for random grain boundaries. The complete wetting of the first GB of the distribution starts at 715 °C [13]. Some of the “special” CSL GBs are completely wetted before all of the random GBs. Their maximal wetting temperatures are marked with small circles. At 825 °C, all random GBs are wetted. All cusps that exist under the line of maximum wetting temperatures of random GBs represent GBs with higher wetting temperatures. The low misorientation angle GBs and the $\Sigma 3$ CSL boundaries do not reach their complete wetting temperature in the temperature range of the two-phase area examined as the line of the low-angle GB does not reach the 0° misorientation and the $\Sigma 3$ lines hit the melting line and do not form a cusp. This means that some of these

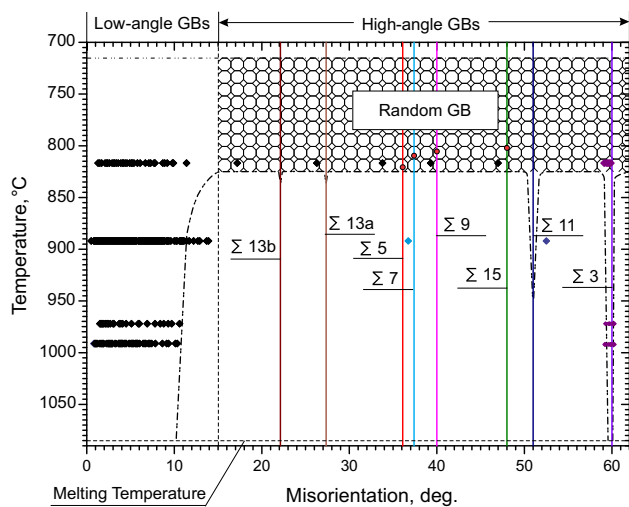


Fig. 6 Wetting temperature observed for different grain boundaries/misorientation angles. The graph is plotted in misorientation in degrees to temperature in °C coordinates and is divided into two parts. In the left part, labelled on the top “low-angle GBs”, we can see the wetting intervals for low-angle GBs. The wetting starts at 715 °C. From 0 to 10° of misorientation, no GB wetting until the melting temperature was found. From 10 to 15° of misorientation the $T_{wfinish}$ value decreases from the melting temperature value of 1084 to 825 °C very fast. The second part, labelled on the top “high-angle GBs”, represents the wetting intervals of high-angle GBs. We can see an area between the parallel lines $T_{wstart} = 715$ °C and $T_{wfinish} = 825$ °C that represent the wetting intervals for random high-angle GBs as well as some of the special CSL GBs (their maximum wetting temperatures are shown by round dots on their lines). The vertical lines represent some of the special CSL GBs. Some of these GBs, like $\Sigma 3$, $\Sigma 11$ and $\Sigma 13a, b$, show cusps that indicate that their maximum wetting temperatures are higher than those of the random high-angle GBs. The solid diamond marks on the diagram represent the experimental points for non-wetted and incompletely wetted GBs to supplement the lines drawn on the diagram

boundaries still remain non-wetted, or incompletely wetted, at the onset of bulk melting. To supplement the fitting that was carried out to obtain the curves plotted in Fig. 6, experimental points representing non-wetted and incompletely wetted GB (solid diamond marks in Fig. 6) were added to the diagram.

The fraction of the non-wetted GBs schematically shown by colour coding on the Cu–In phase diagram in Fig. 7 as well as Fig. 5 illustrates that 95 % of GBs are wetted in a temperature range up to 50 °C above the peritectic temperature and 35 °C above the T_{wmin} . This occupies only 13, 4 and 9,4 % of the whole 373 °C temperature range of the two-phase area of the phase diagram.

Discussion

In the previous work [13], the value T_{wmax} was determined to be 986 °C after analysing the wetting state from BSD and light microscopy pictures. Figure 5 clearly shows that

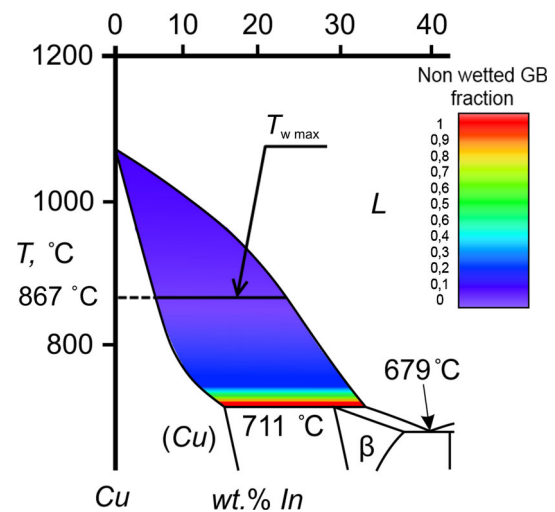


Fig. 7 Schematic representation of the fraction of the non-wetted GBs in colour coding in the phase diagram; from 711 to 800 °C, the colour is changing very fast as most GBs are being wetted in this region; from 800 °C to the melting temperature at 1084 °C, the colour is changing very slowly as the only non-wetted GBs here are the special CSL and low-angle GBs and their wetting temperatures are much higher than the wetting temperatures of all other GBs; the T_{wmax} at 867 °C represents the saturation temperature in Fig. 5 of the “All GBs” line

this value was set too high. The EBSD measurements revealed two error sources such as the low grain contrast and the grain growth due to low quenching rates. Firstly, the low contrast between grains makes the identification of low misorientation angle GBs and $\Sigma 3$ CSL GBs impossible, meaning that they are excluded from the statistics. Secondly, grain growth after slow quenching breaks up the existing liquid film on a GB with a medium energy level making it look like the GB is incompletely wetted. Both of these error sources were successfully overcome in the present work using EBSD.

Based on the diffraction from the crystal structure EBSD gives good contrast between grains of different orientations, and can resolve all low misorientation angle GBs and $\Sigma 3$ CSL GBs present. By analysing the GB shape a decision on whether the GB was wetted or non-wetted at the high temperature can be reached. If it is arc shaped or wave shaped between the triple junctions then it was completely wetted at the high temperature and one of the grains or both grains have grown each into another. If at least a little bit of the GB is straight and is situated on a straight line between the triple junctions then the GB was not completely wetted at the high temperature.

This shows the importance of EBSD analysis for research in the field of GB wetting phase transitions. It is important to mention that in the samples with annealing temperatures from 712 to 750 °C, the quenching rate was high enough and so 95 % of the experimental data in this

work was not effected be the previously described second error source.

The data presented in Fig. 6 allow comparison with plots of grain boundary energy against angular misorientation. As all GBs are wetted with the same In-rich liquid phase, we assume the solid/liquid interfacial energy σ_{SL} to be approximately equal for all solid crystal interfaces contacting the liquid phase. The same assumption is used in GB grooving experiments [30]. Only special planes such as $\{100\}$, $\{110\}$ and $\{111\}$ are likely to have a considerably different σ_{SL} . Assuming that the fraction of these is too low to be significant and, therefore, that the interfacial energy σ_{SL} is equal for all grains, the energy of different GBs can be directly related to their wetting temperatures.

It is clear from Fig. 6 that although a clear classification between “general” and “special” GB in terms of their propensity to wetting can be identified, there is no simple relationship between this “specialness” and the CSL character of the grain boundaries, as determined using the Brandon criterion and seen in literature [25]. Only the $\Sigma 1$ (low-angle), $\Sigma 3$ and $\Sigma 11$ CSL boundaries exhibit clearly identifiable special wetting behaviour. This agrees with the data on the GB energy from other experimental [31] and modelling [32, 33] investigations in pure copper. $\Sigma 7$ CSL GB has a single point in Fig. 6 representing the as yet unconfirmed [33] possibility of special behaviour. Other CSL boundaries (notably $\Sigma 5$ and $\Sigma 9$) are observed to undergo the wetting transition at the same or even lower temperatures than random high misorientation angle GBs. The data for the $\Sigma 9$ CSL GBs supports the previous theoretical assumptions that were based on computer modelling [33]. The absence of the special wetting behaviour of the $\Sigma 5$ CSL GBs can be explained either by the fact that according to the literature [34] the relative energy value of $\Sigma 5$ CSL GBs is not much lower than the energy of general GBs or by the not strict enough Brandon criterion. It should also be noted that the deviations from exact coincidence over which these special properties are observed in CSL boundaries other than $\Sigma 1$ are around $1\text{--}2^\circ$, significantly smaller than the allowed tolerances of the Brandon criterion (8.6° in the case of $\Sigma 3$). These observations, taken together, agree with concerns raised by authors of previous work on the applicability of the Brandon criterion [35, 36] and on the importance of the grain boundary plane in some cases, rather than the CSL character, in determining whether special properties occur [37]. Evidence for the importance of grain boundary plane orientation can be seen, for example, from a closer examination of the incompletely wetted $\Sigma 3$ boundary running approximately diagonally between the central pair of grains in Fig. 8. The boundary forms step-like facets, some of which exhibit lenticular droplets of the wetting phase. Using the Randle plane trace analysis method [38], in which a plane with surface trace

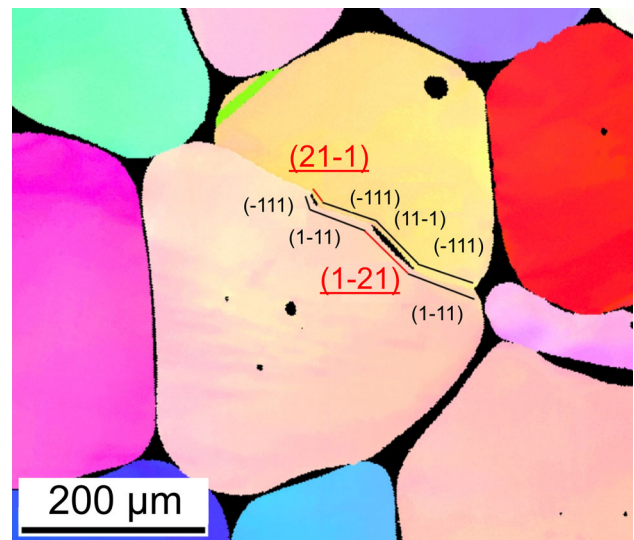


Fig. 8 Stepped $\Sigma 3$ boundary, showing wetted and unwetted sections; $\{111\}$ -type planes that nearly satisfy the Randle plane trace criterion are shown in *black* where these exist; otherwise, the $\{112\}$ -type planes most closely satisfying the Randle criterion are shown with *brighter lines and bigger font*; it is clearly seen that the sections of the $\Sigma 3$ boundary where the $\{111\}$ -type planes in the first grain meet the $\{112\}$ -type planes in the second grain have a much higher energy than the ideal $\Sigma 3$ boundary sections and therefore they are filled with the second wetting phase

vector t can be of type (hkl) if $\hat{t} \cdot \hat{n} = 0$, where n is the normal to the plane (hkl) , the $|\hat{t} \cdot \hat{n}|$ values for the nearest $\{111\}$ (coherent twinning) plane were found for the different sections of the stepped boundary. On both sides, the unwetted sections and on one side of each of the wetted sections, a $\{111\}$ -type plane with a $|\hat{t} \cdot \hat{n}|$ value lower than 0.15; these planes are marked in black in Fig. 8. However, on the other sides of the wetted sections, there was no $\{111\}$ -type plane with a $|\hat{t} \cdot \hat{n}|$ value lower than 0.15. The $\{112\}$ -type plane with the lowest $|\hat{t} \cdot \hat{n}|$ value was instead determined, and these planes are illustrated in red on Fig. 8. It can be seen from this figure that wetting droplets are present on the incoherently twinned boundary sections, i.e. the sections for which the boundary plane is not $\{111\}$ for both the adjoining grains.

Conclusions

The present work has demonstrated that the wide temperature interval between T_{wmin} and T_{wmax} can be attributed to the difference in temperatures associated with wetting of special and general grain boundaries. Special behaviour was found for low-angle, $\Sigma 3$, $\Sigma 11$ (and possibly $\Sigma 7$) GB but not for other CSL boundaries. The commonly used approach (CSL model and Brandon criterion) is therefore incapable of rationalising the difference in

wetting behaviour between general and special boundaries and it is likely that the grain boundary plane orientation plays a significant role in the special or general wetting behaviour of grain boundaries. Further work similar to that in [35] is required to clarify this point.

Acknowledgements The authors want to thank Mrs. Kornelia Strieso and Mr. Norbert Lindner for help in metallographic preparation and SEM measurements. The authors gratefully acknowledge the financial support of the Russian Foundation for Basic Research (Grant 14-08-00972), The Ministry of Education and Science of the Russian Federation in the Framework of Increase Competitiveness Program of MISiS and the Erasmus Mundus Action 2 Programme of the European Union.

References

- German RM, Suri P, Park SJ (2009) Review: liquid phase sintering. *J Mater Sci* 44:1–39. doi:10.1007/s10853-008-3008-0
- Ross D, Bonn D, Meunier J (1999) Observation of short-range critical wetting. *Nature* 400:737–739. doi:10.1038/23425
- Watson EB (1982) Melt infiltration and magma evolution. *Geology* 10:236–240. doi:10.1130/0091-7613(1982)10<236:MIAME>2.0.CO;2
- Laporte D, Watson E (1995) Experimental and theoretical constraints on melt distribution in crustal sources: the effect of crystalline anisotropy on melt interconnectivity. *Chem Geol* 124:161–184. doi:10.1016/0009-2541(95)00052-N
- Straumal B, Gust W (1996) Lines of grain boundary phase transitions in bulk phase diagrams. *Mater Sci Forum* 207–209:59–68. doi:10.4028/www.scientific.net/MSF.207-209.59
- Straumal B, Gust W, Watanabe T (1999) Tie lines of the grain boundary wetting phase transition in the Zn-rich part of the Zn–Sn phase diagram. *Mater Sci Forum* 294–296:411–414. doi:10.4028/www.scientific.net/MSF.294-296.411
- Cahn JW (1977) Critical point wetting. *J Chem Phys* 66:3667–3672. doi:10.1063/1.434402
- Ebner C, Saam W (1977) New phase-transition phenomena in thin argon films. *Phys Rev Lett* 38:1486–1489. doi:10.1103/PhysRevLett.38.1486
- Polyakov SA, Straumal BB, Mittemeijer EJ (2006) Temperature influence on the faceting of $\Sigma 3$ and $\Sigma 9$ grain boundaries in Cu. *Acta Mater* 54:167–172. doi:10.1016/j.actamat.2005.08.037
- Schölhammer J, Baretzky B, Gust W, Mittemeijer E, Straumal B (2001) Grain boundary grooving as an indicator of grain boundary phase transformations. *Interface Sci* 9:43–53. doi:10.1023/A:1011266729152
- Straumal BB, Polyakov SA, Bischoff E, Gust W, Mittemeijer EJ (2001) Faceting of $\Sigma 3$ and $\Sigma 9$ grain boundaries in copper. *Interface Sci* 9:287–292. doi:10.1023/A:1015174921561
- Straumal BB, Klinger LM, Shvindlerman LS (1984) The effect of crystallographic parameters of interphase boundaries on their surface tension and parameters of the boundary diffusion. *Acta Metall* 32:1355–1364. doi:10.1016/0001-6160(84)90081-6
- Straumal AB, Bokstein BS, Petelin AL, Straumal BB, Baretzky B, Rodin AO, Nekrasov AN (2012) Apparently complete grain boundary wetting in Cu–In alloys. *J Mater Sci* 47:8336–8343. doi:10.1007/s10853-012-6773-8
- Kucheev YO, Straumal AB, Mogil'nikova IV, Straumal BB, Gusak AM, Baretzky B (2012) Wetting of grain boundaries in hard-magnetic Nd–Fe–B alloys. *Russ J Non-Ferr Met* 53:450–456. doi:10.3103/S106782121206003X
- Kogtenkova OA, Straumal BB, Protasova SG, Gornakova AS, Zięba P, Czeppe T (2012) Effect of the wetting of grain boundaries on the formation of a solid solution in the Al–Zn system. *JETP Lett* 96:380–384. doi:10.1134/S0021364012180063
- Straumal BB, Kucheev YO, Efron LI, Petelin AL, Majumdar JD, Manna I (2012) Complete and incomplete wetting of ferrite grain boundaries by austenite in the low-alloyed ferritic steel. *J Mater Eng Perform* 21:667–670. doi:10.1007/s11665-012-0130-6
- Straumal BB, Kucheev YO, Yatskovskaya IL, Mogilnikova IV, Schütz G, Nekrasov AN, Baretzky B (2012) Grain boundary wetting in the NdFeB-based hard magnetic alloys. *J Mater Sci* 47:8352–8359. doi:10.1007/s10853-012-6618-5
- Straumal BB, Gornakova AS, Kucheev YO, Baretzky B, Nekrasov AN (2012) Grain boundary wetting by a second solid phase in the Zr–Nb alloys. *J Mater Eng Perform* 21:721–724. doi:10.1007/s11665-012-0158-7
- Wynblatt P, Takashima M (2001) Correlation of grain boundary character with wetting behaviour. *Interface Sci* 9:265–273. doi:10.1023/A:1015162929100
- Wynblatt P, Takashima M (2001) An empirical model of grain boundary energy and its application to grain boundary wetting. *Trans JWRI* 30:11–21
- Felberbaum L, Rossoll A, Mortensen A (2005) A stereoscopic method for dihedral angle measurement. *J Mater Sci* 40:3121–3127. doi:10.1007/s10853-005-2673-5
- Empl D, Felberbaum L, Laporte V, Chatain D, Mortensen A (2009) Dihedral angles in Cu–1 wt% Pb: grain boundary energy and grain boundary triple line effects. *Acta Mater* 57:2527–2537. doi:10.1016/j.actamat.2009.02.009
- Kronberg ML, Wilson FH (1949) Secondary recrystallization in copper. *Trans AIME* 185:501–514
- Brandon D (1966) The structure of high-angle grain boundaries. *Acta Metall* 14:1479–1484. doi:10.1016/0001-6160(66)90168-4
- Shvindlerman L, Straumal B (1985) Regions of existence of special and non-special grain boundaries. *Acta Metall* 33:1735–1749. doi:10.1016/0001-6160(85)90168-3
- Straumal B, Muschik T, Gust W, Predel B (1992) The wetting transition in high and low energy grain boundaries in the Cu (In) system. *Acta Metall Mater* 40:939–945. doi:10.1016/0956-7151(92)90070-U
- Massalski TB (ed) (1990) Binary alloy phase diagrams. ASM International, Materials Park
- Polkowski W, Józwick P, Polański M, Bojar Z (2013) Microstructure and texture evolution of copper processed by differential speed rolling with various speed asymmetry coefficient. *Mater Sci Eng* 564:289–297. doi:10.1016/j.msea.2012.12.006
- Adams BL, Wright SI, Kunze K (1993) Orientation imaging: the emergence of a new microscopy. *Metal Trans A* 24:819–831. doi:10.1007/BF02656503
- Protsenko P, Kucherinenko Y, Robaut F, Traskine V, Eustathopoulos N (2003) Misorientation effects on grain boundary grooving of Ni by liquid Ag. *Def Diffus Forum* 216–217:225–230. doi:10.4028/www.scientific.net/DDF.216-217.225
- McLean M (1973) Grain-boundary energy of copper at 1030 °C. *J Mater Sci* 8:571–576. doi:10.1007/BF00550462
- Takata N, Ikeda K, Yoshida F, Nakashima H, Abe H (2004) Grain boundary structure and its energy of symmetric tilt boundary in copper. *Mater Sci Forum* 467–470:807–812. doi:10.4028/www.scientific.net/MSF.467-470.807
- Weckman AV, Dragunov AS, Dem'yanov BF, Adarich NV (2012) Energy spectrum of tilt grain boundaries in copper. *Russ Phys J* 55:799–806. doi:10.1007/s11182-012-9883-5
- Mori T, Miura H, Tokita T, Haji J, Kato M (1988) Determination of the energies of [001] twist boundaries in Cu with the shape of boundary SiO₂ particles. *Philos Mag Lett* 58:11–15. doi:10.1080/09500838808214724

35. Palumbo G, Aust KT, Lehockey EM, Erb U, Lin P (1998) On a more restrictive geometric criterion for “special” CSL grain boundaries. *Scr Mater* 38:1685–1690. doi:[10.1016/S1359-6462\(98\)00077-3](https://doi.org/10.1016/S1359-6462(98)00077-3)
36. King AH, Shekhar S (2006) What does it mean to be special? The significance and application of the Brandon criterion. *J Mater Sci* 41:7675–7682. doi:[10.1007/s10853-006-0665-8](https://doi.org/10.1007/s10853-006-0665-8)
37. Randle V (2006) ‘Special’ boundaries and grain boundary plane engineering. *Scr Mater* 54:1011–1015. doi:[10.1016/j.scriptamat.2005.11.050](https://doi.org/10.1016/j.scriptamat.2005.11.050)
38. Randle V (2001) A methodology for grain boundary plane assessment by single-section trace analysis. *Scr Mater* 44:2789–2794. doi:[10.1016/S1359-6462\(01\)00975-7](https://doi.org/10.1016/S1359-6462(01)00975-7)